

*Chapter 3*ACTIVITY OF A PY-IM POLYAMIDE TARGETED
TO THE ESTROGEN RESPONSE ELEMENT

The text of this chapter was taken in part from a manuscript co-authored with Nicholas G. Nickols, Amanda E. Hargrove, Benjamin C. Li, Jevgenij A. Raskatov, and Peter B. Dervan.

(Nickols NG*, **Szablowski JO***, Hargrove AE, Li BC, Raskatov JA, Dervan PB. "Activity of a Py-Im Polyamide Targeted to the Estrogen response Element," *Mol. Cancer Ther.*, **12**:675-684, (2013).

*denotes equal contribution)

Abstract

Pyrrole-imidazole (Py-Im) polyamides are a class of programmable DNA minor groove binders capable of modulating the activity of DNA-binding proteins and affecting changes in gene expression. Estrogen receptor alpha (ER α) is a ligand-activated hormone receptor that binds as a homodimer to estrogen response elements (ERE) and is a driving oncogene in a majority of breast cancers. We tested a selection of structurally similar Py-Im polyamides with differing DNA sequence specificity for activity against 17 β -estradiol (E2)-induced transcription and cytotoxicity in ER α positive, E2-stimulated T47DKBluc cells, which express luciferase under ER α control. The most active polyamide targeted the sequence 5'-WGGWCW-3' (W = A or T), which is the canonical ERE half site. Whole transcriptome analysis using RNA-Seq revealed that treatment of E2-stimulated breast cancer cells with this polyamide reduced the effects of E2 on the majority of those most strongly affected by E2, but had much less effect on the majority of E2-induced transcripts. *In vivo*, this polyamide circulated at detectable levels following subcutaneous injection and reduced levels of ER-driven luciferase expression in xenografted tumors in mice after subcutaneous compound administration without significant host toxicity.

Estrogen receptor-alpha ($ER\alpha$) is a member of the nuclear hormone receptor family of transcription factors and is active in a majority of breast adenocarcinomas (1, 2). Breast tumors that express $ER\alpha$ and are sensitive to circulating estrogens respond to therapeutics that modulate $ER\alpha$ activity (3). Such therapeutics include tamoxifen, a selective ER modulator that acts as a weak agonist/antagonist by binding to the $ER\alpha$ ligand-binding pocket and the aromatase inhibitors that inhibit synthesis of E2 (3). A different strategy for modulation of $ER\alpha$ activity is inhibition of the $ER\alpha$ -ERE interface by a DNA-binding molecule.

Pyrrole-imidazole (Py-Im) polyamides are a class of synthetic, minor groove-binding ligands inspired by the natural product distamycin A (4, 5). Py-Im polyamides are oligomers of aromatic amino acids linked in series to fold in an antiparallel fashion when bound in the minor groove of DNA (4, 5). Sequence specificity is programmed through side-by-side pairings of the Py and Im subunits that recognize differences in the shape and hydrogen bonding pattern presented by the edges of the Watson-Crick base pairs in the floor of the minor groove (6, 7). Binding specificity has been extensively characterized by DNase I footprinting titrations and other methods. An Im:Py pair preferentially recognizes G:C; Py:Im prefers C:G, and Py:Py is degenerate for A:T and T:A (6, 7). Py-Im polyamide binding in the minor groove also induces allosteric changes to the major groove (8, 9), and binding affinity is sufficient to modulate the binding of DNA-binding proteins (8-11).

In cell culture, selected polyamides have been used to modulate expression of genes induced by testosterone (11), TNF- α (12), hypoxia (13, 14), and dexamethasone (10). The mechanisms by which polyamides affect gene expression changes in cell culture are still

not well understood and may involve direct effects on multiple DNA-dependent processes including transcription factor occupancy, chromatin structure, RNA polymerases, and DNA replication (15). The pharmacokinetics and toxicity of a number of polyamides after intravenous and subcutaneous injection in mice and rats have been described (16–18). In mice, a selected polyamide was reported to induce changes in TGF- β expression in kidney glomeruli, and a fluorescent analog of this polyamide was observed in kidney glomeruli after tail vein injection in rats (19). Gene expression changes have also been observed in tumor xenografts in immune-compromised mice treated with a hairpin-polyamide (20).

In this study, our goal was to identify a Py-Im polyamide capable of affecting E2-stimulated gene expression in breast cancer cells and characterize its activity in cell culture and in tumor xenografts. To do this, we drew from an earlier study that reported a polyamide targeted to the estrogen response element (ERE) consensus half site 5'-WGGWCW-3' inhibited ER α -binding to DNA in cell-free systems (21). The DNA-binding affinity and specificity of the ERE-targeted polyamide was characterized in this and other studies (21, 22). Since those publications, we have improved the nuclear uptake of polyamides via modification of the C-terminus (23). We have also shown that polyamides are bioavailable after intravenous and subcutaneous injection in mice (20, 24). We then decided to reexamine the activity of polyamides capable of disrupting ERE-driven gene expression for use *in vivo*. We have screened a focused library of polyamides for cytotoxicity and inhibition of luciferase activity using the breast cancer cell line T47D-KBluc that expresses luciferase under the control of 3 tandem, canonical EREs (25). The most active polyamide identified, which targets the consensus ERE, was further evaluated

and showed a partial suppression of E2-stimulated gene expression in cell culture. This polyamide circulated in mouse serum after subcutaneous injection and showed activity against E2-induced luciferase expression in T47D-KBluc tumor xenografts in mice with minimal host toxicity. A fluorescent analog of this polyamide distributed widely in both tumor and mouse tissue after subcutaneous injection.

Materials and Methods

Polyamide synthesis and characterization

The polyamides **1** to **5** were synthesized following previously published solid phase synthesis protocols (26). Compound purities were confirmed by analytic high-performance liquid chromatography (HPLC) and matrix-assisted laser desorption/ionization–time-of-flight (MALDI-TOF) mass spectrometry. Melting temperature analysis was conducted on a Varian Cary 100 spectrophotometer with temperature control. Oligonucleotides (IDTDNA) were dissolved in 10 mmol/L sodium cacodylate, 10 mmol/L KCl, 10 mmol/L MgCl₂, and 5 mmol/L CaCl₂ at pH 7.0 at a concentration of 2 μmol/L. Polyamides were added to oligo solution to a final concentration of 4 μmol/L in 0.1% dimethyl sulfoxide (DMSO). Oligonucleotides were annealed from 25°C to 90°C and then back to 25°C at 5°C/min. Subsequently, the temperature was elevated at a rate 0.5°C/min between 25°C and 90°C. Melting temperatures are defined as a maximum of the first derivative of absorbance at 260 nm over the range of temperatures.

Cell culture and imaging

Cell lines used were purchased directly from American Type Culture Collection (ATCC) and used within 6 months. No subsequent authentications were done by the authors. All

experiments were carried out with T47D-KBluc cells (ATCC), unless specifically mentioned otherwise. Cells were grown in RPMI-1640 and held at 37°C in 5% CO₂. Media was supplemented with 10% FBS and 1% penicillin/streptomycin. Before imaging, cells were plated in 35-mm optical dishes (MatTek) at 5×10^4 cells per dish in the presence of 10 nmol/L E2. Cells were dosed with polyamide for 24 hours. Cells were then washed twice with PBS and imaged on a confocal microscope (Exciter, Zeiss) using a $\times 63$ oil immersion lens in a method previously described. Confocal imaging was conducted following our previously published protocols (27, 28).

Tissue processing for fluorescence imaging

The tissue sections for fluorescent imaging were obtained by fixing the tumors in 10% formaldehyde solution for 24 hours and subsequent cryoprotection in 15% sucrose (24 hours) and 30% sucrose (24 hours). The tumors were frozen in Tissue-Tek O.C.T. (Sakura Finetek) and 50 μm (for T47D-KBluc xenograft) or 10 μm (for other tissues) sections were obtained using a Leica CM 1800 cryotome. Imaging was conducted as described earlier.

Cell toxicity and luciferase assays

T47D-KBluc cells were plated at 3×10^3 cells per well in 96-well plates, incubated in standard growth media containing 10 nmol/L E2 for 48 hours, and then dosed with medium containing 10 nmol/L E2 and between 2 nmol/L and 50 $\mu\text{mol/L}$ polyamides. The cells were then incubated for 96 hours and analyzed using either WST-1 assay (Roche) or luciferase assay system (Promega) according to the manufacturers' instructions.

Gene expression analysis by qRT-PCR

Cells were plated in 12 well-plates at 1.1×10^5 cells/well and incubated in the growth medium supplemented with 10 nmol/L E2 for 24 hours. Afterward, medium was exchanged with the growth medium supplemented with polyamides and 10 nmol/L E2. Quantitative real-time PCR (qRT-PCR) was conducted according to previously established protocols (3–6). Confirmation of inhibition of *TFF1* expression by polyamides 1 to 4 was carried out and qRT-PCR was conducted following the same timeline as cell toxicity and luciferase assays. Gene expression was normalized against *GUSB* as a housekeeping gene. All primers yielded single amplicons as determined by both melting denaturation analysis and agarose gel electrophoresis. The following primer pairs were used. *GUSB*: forward 5'-CTC ATT TGG AAT TTT GCC GAT T-3'; reverse 5'-CCC AGT GAA GAT CCC CTT TTT A-3'. *DOK7*: forward 5'-GAC AAG TCG GAG CGT ATC AAG-3'; reverse 5'-ATG TCC TCT AGC GTC AGG CT-3'. *WT1*: forward 5'-CAC AGC ACA GGG TAC GAG AG-3'; reverse 5'-CAA GAG TCG GGG CTA CTC CA-3. *TGFB2*: forward 5'-CAG CAC ACT CGA TAT GGA CCA-3'; reverse 5'-CCT CGG GCT CAG GAT AGT CT-3'.

Chromatin immunoprecipitation experiments

T47D-KBluc cells were plated into 500-cm² plates and grown in RPMI-1640 with 10% FBS until 75% confluence was reached. Plates were washed with RPMI-1640 with charcoal-treated 10% FBS, and then the media was replaced with RPMI-1640 with charcoal-treated 10% FBS with 2 μ mol/L polyamide 1 and incubated for 48 hours. Plates were then treated with 10 nmol/L E2 or vehicle for 45 minutes. Cross-linked chromatin was obtained using the 2-step cross-linking methods previously described (29). Chromatin

was isolated and sheared. Antibodies to ER α (AC-066-100; Diagenode) were used to immunoprecipitate ER α -bound DNA fragments. Cross-links were reversed and PCRs using primers targeted to the regions of interest were used to assess enrichment of bound fragments as compared with negative controls. *TFF1* promoter: forward 5'-TCA GAT CCC TCA GCC AAG AT-3'; reverse 5'-TGG TCA AGC TAC ATG GAA GG-3'. Negative loci control: forward 5'-AAA GAC AAC AGT CCT GGA AAC A-3'; reverse 5'-AAA AAT TGC TCA TTG GAG ACC-3'.

Circulation and toxicity in vivo

All animal experiments were carried out according to approved Institutional Animal Care and Use Committee protocols at the California Institute of Technology (Pasadena, CA). Circulation studies were done as previously described (30). Briefly, 120 nmol of polyamide 1 was injected subcutaneously into the right flank of 4 female C57BL/6 mice in a total of 200 μ L of a 20% DMSO/PBS vehicle. Blood was collected retroorbitally at serial time points. Serum was treated with methanol, analyzed via HPLC, and quantified against a standard curve of concentration versus peak area, all as previously described, to determine approximate serum concentrations (24). For toxicity studies, 5 female C57BL/6 mice were injected with 20 nmol of polyamide 1 in a total of 200 μ L of a 20% DMSO/PBS vehicle on days 1, 3, 5, 8, 10, 12, and then with 30 nmol on days 15, 17, 19, 22, 24, and 26 and were weighed before each treatment day. Mice were euthanized if weight loss was more than 15% of initial body weight, if dehydration was more than 10%, or if moribund behavior was observed. None were observed in this experiment.

Engraftment of T47D-KBluc.

Experiments were carried out in appropriately shaved female NSG mice (JAX) between 8 and 12 weeks of age. Cells were injected into the left flank area of the animals as suspensions of $5.0 \times 10^6 \text{ mL}^{-1}$ in 50% RPMI-1640 growth medium and 50% Matrigel, 200 μL per injection. Mice also received a subcutaneous E2 pellet (0.72 mg, 60-day slow release; Innovative Research of America) implanted into the right flank on the day of engraftment.

Treatment and tumor monitoring.

Mice were treated with either 25 nmol of polyamide 1 or 50 nmol of polyamide 5. For the short-term and fluorescent imaging studies, they were treated for 8 days after engraftment and every second day for a total of 4 injections. For long-term treatment, injections started 16 days after engraftment and were continued twice a week for the following 4 weeks. Imaging was accomplished using the IVIS Imaging System (Caliper). The animals were anesthetized with 2% to 3% isoflurane and injected intraperitoneally with 150 μL of RediJect D-luciferin (Caliper) and subsequently transferred to the imaging chamber, where isoflurane levels were reduced to 1% to 2.5%. The floor of the imager was heated to $+37^\circ\text{C}$ to avoid animal hypothermia. Breathing frequency was monitored and not allowed to drop below 1 per second, adjusting the isoflurane levels accordingly at all times.

Endpoint criteria and euthanasia.

Animal endpoint criteria encompassed weight loss of more than 15%, restriction of motoric function by the engrafted tumor, dehydration of more than 10%, and moribund behavior. Where appropriate, the animals were euthanized by asphyxiation in a CO_2 chamber.

Tumor tissue harvest.

Animals were resected and tumors excised using standard forceps, scissors, and surgical blades. The tumors were weighed immediately afterward. For studies with fluorescein isothiocyanate (FITC)-conjugate 5, resected tumor tissue was homogenized via blunt force and then pushed through a microfilter to achieve single cell suspensions, which were plated on glass microscopy slides for 6 hours before imaging using a Zeiss Exciter fluorescence confocal microscope.

RNA-Seq sample preparation and data processing

Cells for gene expression analysis were plated in 10-cm diameter dishes at 1.1×10^6 cells per dish and incubated in the growth medium supplemented with 10 nmol/L E2 for 24 hours. Afterward, medium was exchanged with the growth medium supplemented with polyamides and 10 nmol/L E2 and incubated for 48 hours in 5% CO₂ and 37°C. The RNA was then harvested using an RNEasy Kit (Qiagen). Subsequently, a Riboguard RNase inhibitor was added and samples were treated with TurboDNA Free DNase (Ambion), according to manufacturers' instructions. RNA-Seq libraries were prepared using standard Illumina reagents and protocols. Single read sequencing with the read length of 50 nucleotides were conducted on the Illumina HiSeq2000 sequencer, following manufacturers' instructions, producing 35 to 50 million reads per library. Sequencing data were mapped against the combined human (hg19) transcriptome, using the Bowtie program package 0.12.7 (31) and the refseq annotation. The open access processing package Cuffdiff was used to calculate differential gene expression. Inter-replicate statistical significance was calculated with the DEseq module (32).

Results

Design of polyamides

We synthesized 4 8-ring hairpin Py–Im polyamides to screen for activity against E2-stimulated gene expression (Fig. 3.1 and Fig. 3.2). Polyamide 1 targets 5'-WGGWCW-3', which is the half site ERE consensus. Polyamide 2 was previously reported to inhibit a subset of dihydrotestosterone-induced gene expression in cultured prostate cancer cells (11). Polyamide 3 was recently characterized in cultured lung cancer cells and used to partially abrogate TNF-stimulated transcription (12). Polyamide 4 targets the sequence 5' WGWCGW-3'. Polyamides 5 and 6 are FITC-conjugated analogs of polyamides 1 and 2, respectively, used to visualize cellular uptake and distribution in this study.



Figure 3.1 Ball-and-stick models of polyamides 1 to 6 with DNA target sequences as follows: 1, 5'-WGGWCW-3'; 2, 5'-WGWWCW-3'; 3, 5'-WGGWWW-3'; 4, 5'-WGWCGW-3'. Polyamides 5 and 6 are FITC-analogs of polyamides 1 and 2, respectively, used for fluorescence microscopy experiments. Chemical structures of polyamides 1 to 6 are in Fig. 3.2. IPA, isophthalic acid.

Evaluation of binding of polyamides to an ERE half site by DNA thermal denaturation assays

Polyamides 1 to 4 were incubated with duplex DNA 5'-CGATGGTCAAGC-3', which contains an ERE half site consensus and melting temperatures measured (Fig. 3.3A). Duplex stabilization was greatest for polyamide 1, a polyamide that was predicted to bind this sequence based on established Py-Im polyamide pairing rules (6, 7). The other polyamides showed less stabilization of this duplex.

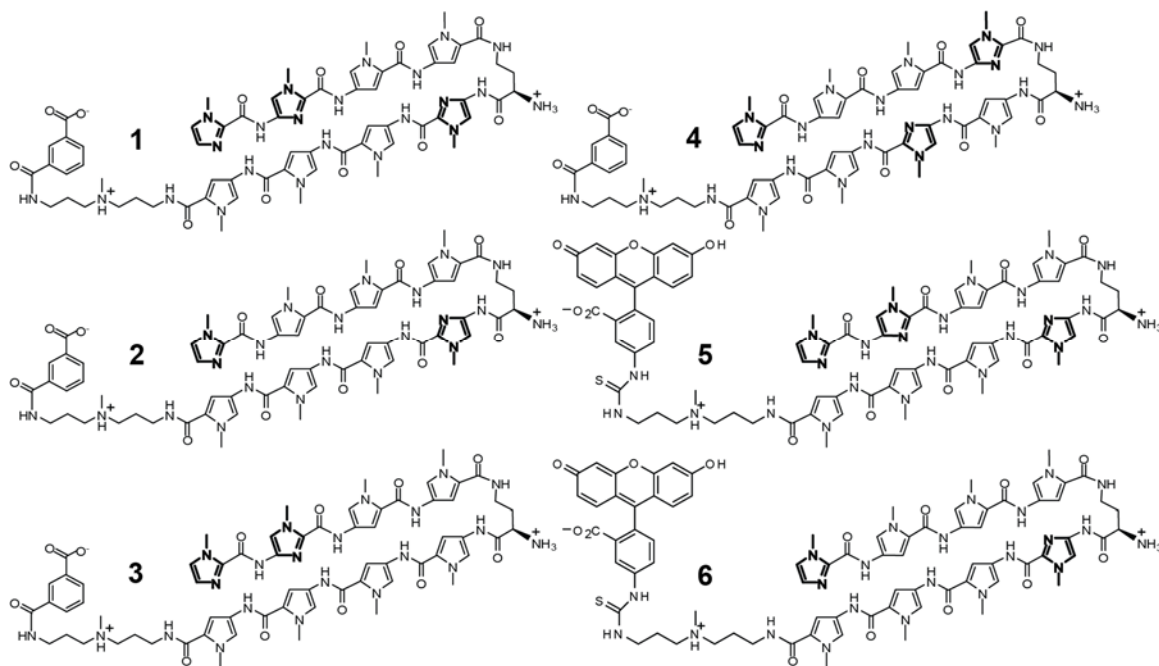


Figure 3.2 Chemical structures of compounds 1-6.

Luciferase activity and cytotoxicity in T47D-KBluc cells

The ER α -positive cell line T47D-KBluc expresses luciferase under the control of 3 tandem repeats of the sequence 5'-AGGTCACCTTGACCT-3' (25), which is the consensus sequence for the ER α -DNA homodimer (Fig. 3.3B). T47D-KBluc cells were grown in 10% FBS/RPMI-1640 media with 10 nmol/L E2 for 48 hours. Then, media was replenished with varying concentrations of polyamides 1 to 4 for 96 hours. An extended incubation time with E2 was used to approximate the *in vivo* condition of continued E2 circulation. Cell proliferation and viability was assayed using WST-1 (Roche) and luciferase output was measured (Fig. 3.3C). Both luciferase output and proliferation were affected most by treatment with polyamide 1 (IC₅₀ 0.47 μ mol/L for viability, 0.14 μ mol/L for luciferase suppression) and least by polyamide 3 (IC₅₀ > 2.5 and 1.5 μ mol/L, respectively). The representative data for luciferase and WST-1 assay are shown in Fig. 3.4. We identified *TFF1* as one of the most highly induced transcripts by E2 based on published reports (33). The effects of polyamides 1 to 4 on E2-stimulated *TFF1* expression were measured to validate the luciferase screen. Polyamide 1 was again found most potent although polyamides 2 and 4 showed significant inhibition of *TFF1* as well (Fig. 3.3D). In addition, polyamide 1 shows significantly less toxicity to LNCaP, U251, and A549 cell lines (Fig. 3.5), which have low expression of ER α (34–37). Inhibition of *TFF1* mRNA by polyamide 1 is dose responsive (Fig. 3.6A) and chromatin immunoprecipitation of ER α at the *TFF1* promoter after E2 stimulation of cells pretreated with **1** showed reduced occupancy as compared with vehicle-treated cells (Fig. 3.6B, C).

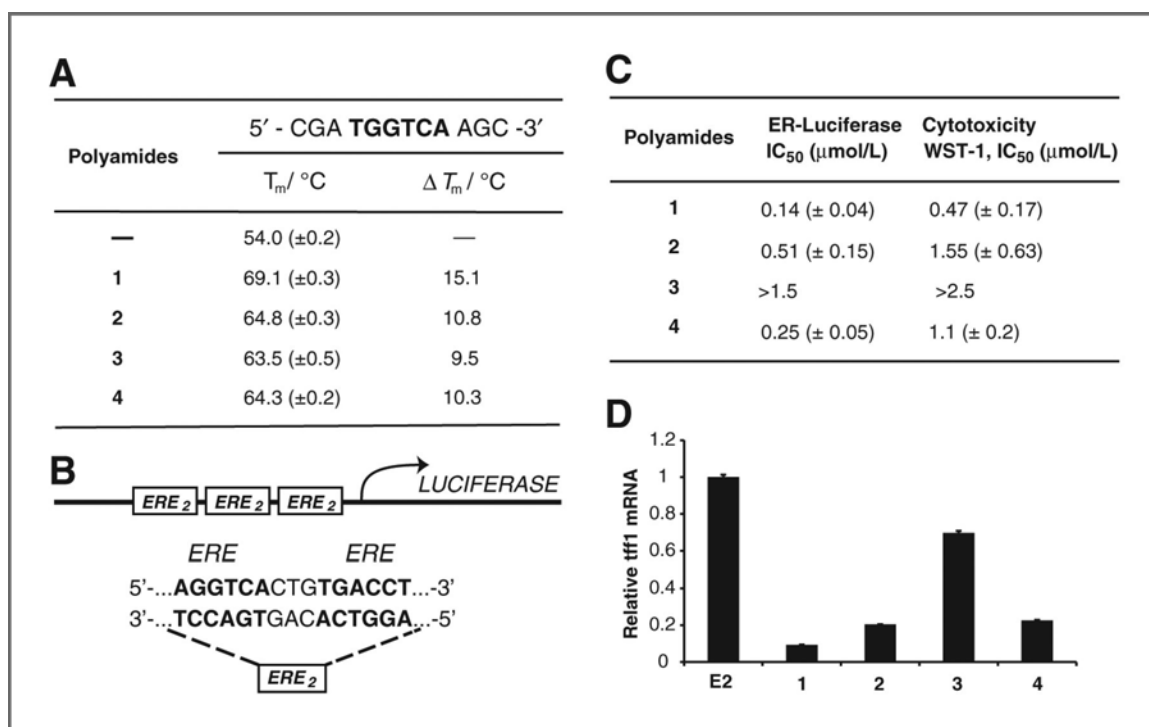


Figure 3.3 A, thermal denaturation assays of a duplex DNA oligonucleotide containing a half site ERE. Polyamide 1 shows the most stabilization. B, sequence of ERE-driven luciferase in T47D-KBLUC cells. C, polyamides 1 to 4 were screened for cytotoxicity and suppression of ER-driven luciferase. Polyamide 1 is most potent by both measures. Representative isotherms are displayed in Fig. 3.4. D, polyamides dosed at 0.3 $\mu\text{mol/L}$ were screened for activity against TFF1 expression, a known ERE-driven gene. The relative activities of polyamides 1 to 4 approximately mirror what is seen in the luciferase assay at this concentration. At higher concentrations ($\sim 1 \mu\text{mol/L}$), all four polyamides show activity.

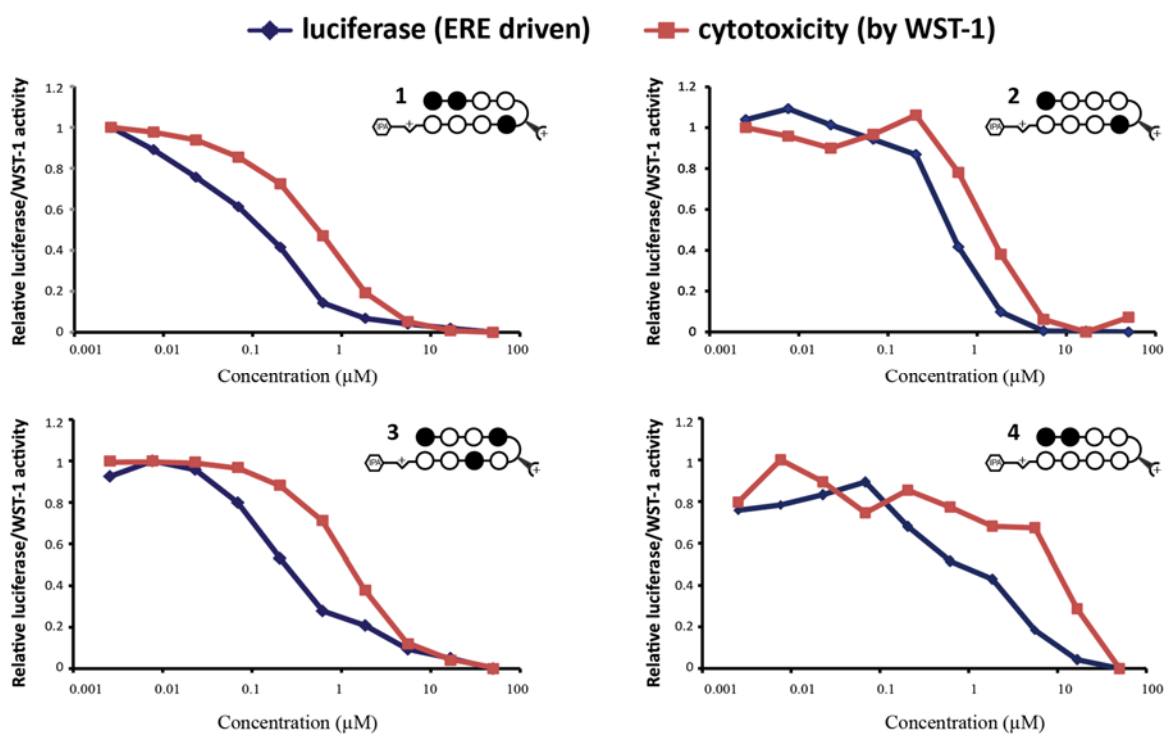


Figure 3.4. Representative data from luciferase and cytotoxicity (wst-1) assays for compounds 1-4.

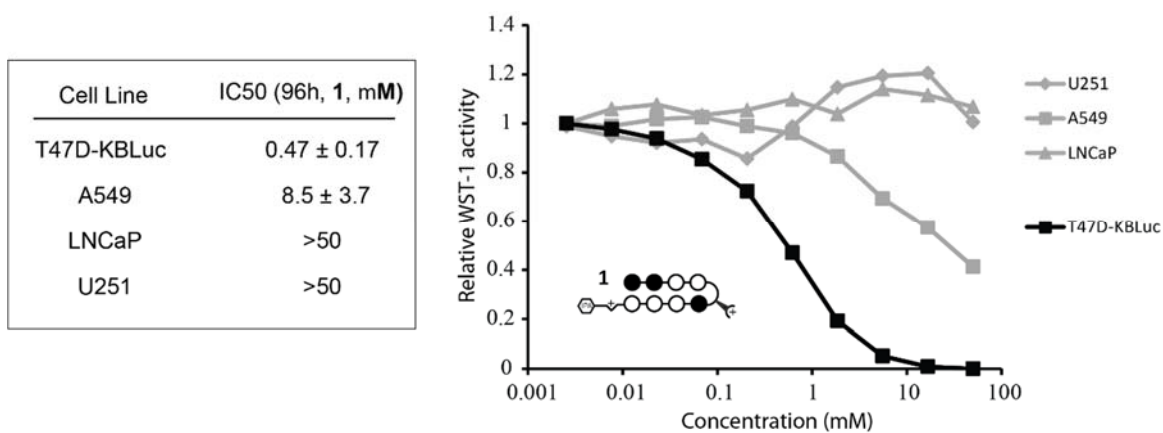


Figure 3.5 WST-1 cytotoxicity of 1 in T47D-KBLUC, LNCaP, A549, and U251 cells.

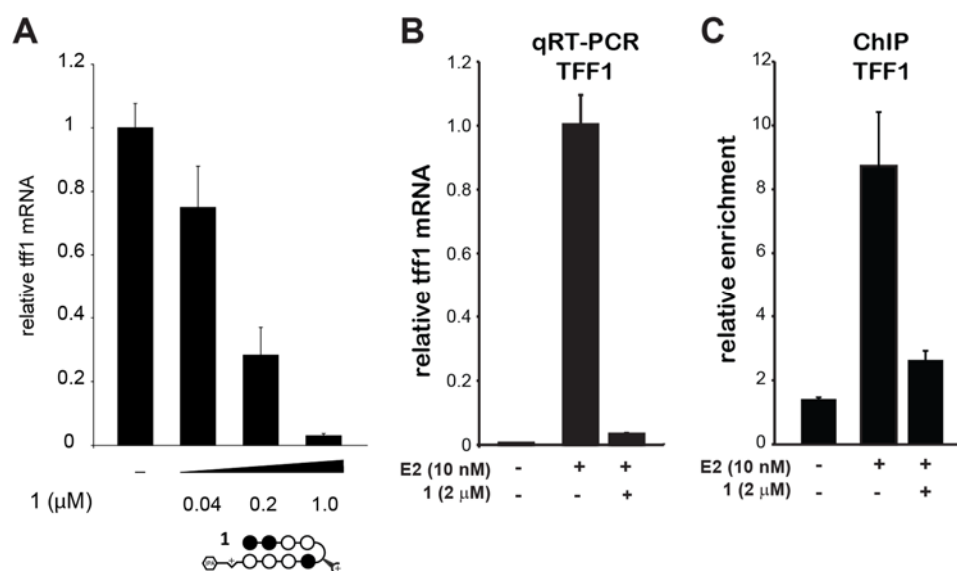


Figure 3.6 Quantitative RT-PCR analysis of Tff1 mRNA reduction after treatment with 1 for 96h is dose responsive. B, Relative mRNA of E2 induced tff1 in the presence of 1 at 2 μM C, ERα occupancy at the tff1 promoter is reduced by 1. The cells were incubated with 1 for 48 hours prior to induction with E2 (10 nM) for 45 minutes. The IC50 for cytotoxicity of 1 at 48h in 10% CT-FBS/RPMI is 3.4 μM.

Genome-wide polyamide effects on E2-induced gene expression

Effects of hairpin polyamide 1 at 0.3 and 1 μmol/L on the transcriptome of E2-induced cells were measured using RNA-Seq. Reads were mapped using Hg19 reference human genome and data were analyzed using the Bowtie and CuffDiff packages (38). Only the genes with fragments per kilobase of exon per million fragments mapped (FPKM) ≥ 20 and at least 2-fold change in gene expression upon treatment with either polyamide 1 or E2 were used in the analysis (Table 3.1). Among those genes, at 1.0 μmol/L, polyamide 1 affected expression of 346 genes (0.7% of total) at least 2-fold as compared with E2-treated control. Of these genes, an equal number of genes were up- and downregulated (173 in each case). At the lower concentration of 0.3 μmol/L, expression of 127 genes (0.3% of total) was affected at least 2-fold, and a majority of these genes (77 vs. 50) were

downregulated. At the same threshold, E2 upregulated 1,003 genes (2.0%; Fig. 3.7A) and downregulated 575 genes (1.2%; Fig. 3.7B). A fraction of expression changes induced by E2 were reversed by polyamide 1 (Table 3.2), and this fraction was greater for E2-repressed genes. Among E2-upregulated genes, 43 (4.3%) were repressed by polyamide 1 at least 2-fold at 1.0 $\mu\text{mol/L}$. Among those 575 genes that were downregulated by E2, 95 (16.5%) were derepressed by 1 at 1.0 $\mu\text{mol/L}$ at least 2-fold (Fig. 3.7A and B). Overall, of the 346 genes affected by polyamide 1 at 1.0 $\mu\text{mol/L}$, 138 (39.9%) represent genes whose up- or downregulation by E2 was abrogated by polyamide treatment. Genes whose expression was affected by polyamide 1 at a lower concentration (0.3 $\mu\text{mol/L}$) were largely a subset of the genes affected at 1.0 $\mu\text{mol/L}$, 103 of which (81.1%) were affected by polyamide 1 at both concentrations.

Further analysis was conducted using Euclidian distance clustering with complete linkage (Fig. 3.7C). Interestingly, while the majority of E2-affected genes are not affected by polyamide 1, out of the top 50 genes most strongly affected by E2, 28 (56%) are inhibited at least 2-fold and 38 of 50 (78%) genes are inhibited at least 1.5-fold by polyamide 1 (Fig. 3.7D). Five transcripts were selected for verification by qRT-PCR and all five showed good reproducibility of the expression changes seen by RNA-Seq (Fig. 3.8). Four were upregulated by E2 (*AREG*, *DOK7*, *TFF1*, and *WT1*) and one downregulated by E2 (*TGFB2*).

Circulation and toxicity of polyamide 1 in mice

To assess serum concentrations of 1 after subcutaneous injection, 4 female C57BL/6 mice were injected subcutaneously into the left flank with 120 nmol of polyamide 1 in a

200 μL 20% DMSO/PBS vehicle. Serial serum samples were taken via retroorbital draw and processed by methods previously described (30). Polyamide 1 was detectable in serum for up to 24 hours after injections, and reached a maximum concentration of 3 $\mu\text{mol/L}$ at 6 hours after injection (Fig. 3.9A). Toxicity after repeated injections of **1** was assessed by daily weights and visual inspection of treated mice. Five female C57BL/6 mice were injected with 20 nmol of polyamide 1 subcutaneously to the left flank 3 times a week for 2 weeks without measurable weight loss. The regimen was then increased to 30 nmol for 2 weeks, again without measurable weight loss or changes in animal behavior (Fig. 3.9B).

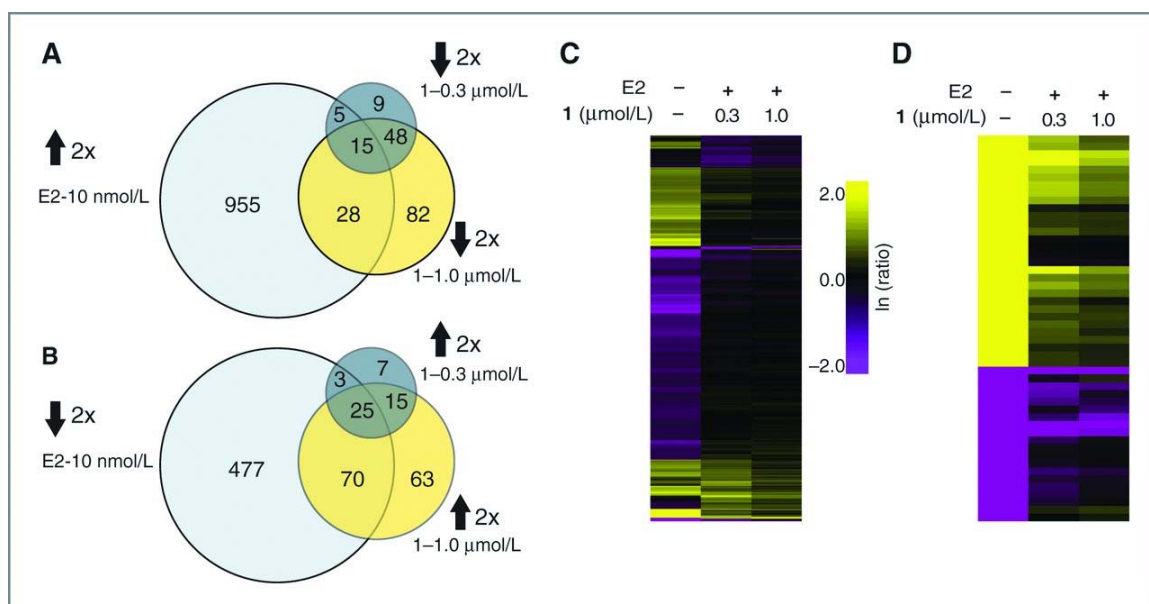


Figure 3.7 RNA-seq global transcriptome analysis. All ratios are normalized to the induced control (10 nmol/L E2). A, Venn diagrams show the overlap between genes upregulated by E2 at least 2-fold and genes downregulated by polyamide 1 at 0.3 or 1.0 $\mu\text{mol/L}$. B, Venn diagrams for the overlap of genes downregulated by E2 at least 2-fold and derepressed by polyamide 1 at 0.3 or 1.0 $\mu\text{mol/L}$. C, hierarchical clustering (Euclidian distance, complete linkage) of genes changed at least 2-fold as compared with the induced state. D, 50 genes that were most changed by E2 induction were clustered (Euclidian distance, complete linkage). Of those genes, 30 were upregulated and 20 were downregulated by E2. Fold-changes are relative to E2-induced control.

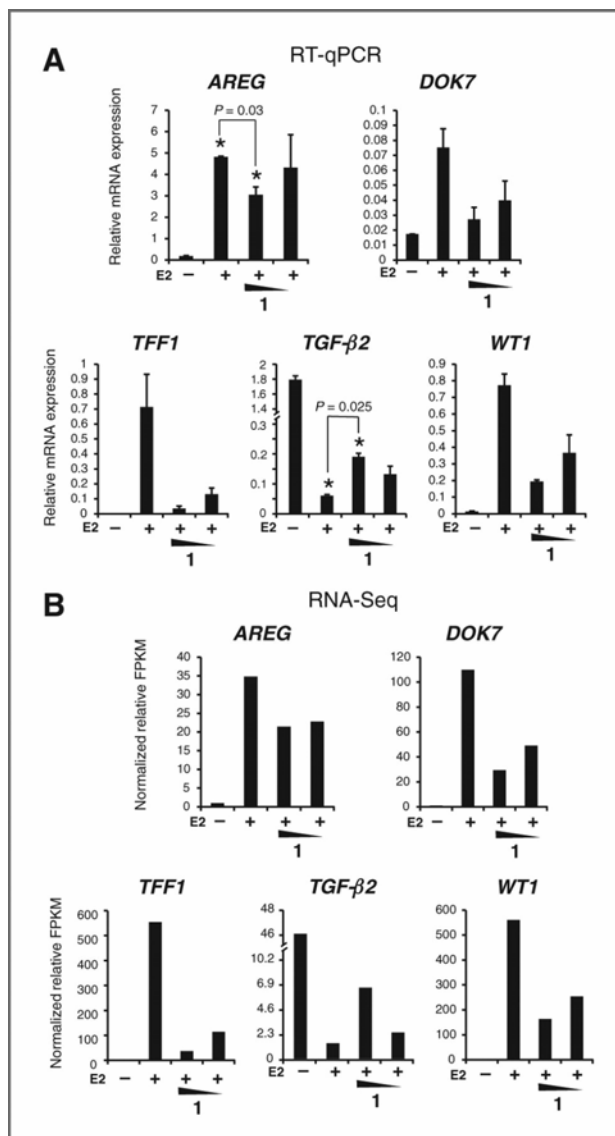


Figure 3.8 Confirmation of genome-wide polyamide effects observed by RNA-seq. Five genes (4 induced and 1 repressed by estrogen) were interrogated. A, relative mRNA levels of selected genes measured by qRT-PCR. B, relative mRNA expression values as measured by FPKM from RNA-seq. Concentrations of polyamide 1 are 1.0 and 0.3 $\mu\text{mol/L}$.

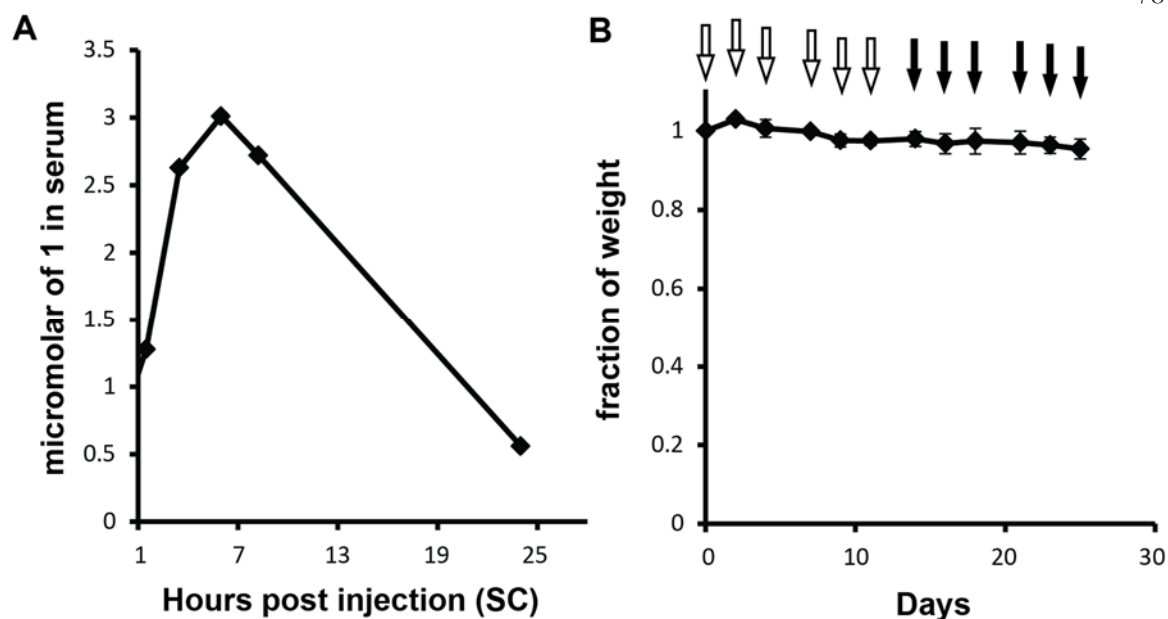


Figure 3.9 Pharmacokinetics of **1**. A, Serum concentrations of **1** after subcutaneous injection (120 nmol) into C57BL/6 mice. B, Weight curves after indicated injections of **1**. Gray arrows: 20 nmol, Black arrows: 30 nmol. n = 4 mice.

Effects on ER α -mediated transcription in T47D-KBluc tumor bearing mice after short-term treatment

To measure the efficacy of polyamide **1** *in vivo* against E2-induced transcription, T47D-KBluc cells were engrafted into female nonobese diabetic/severe combined immunodeficient (NOD/SCID)-gamma (NSG) immunocompromised mice supplemented with a slow-release subcutaneous E2 pellet in the right flank to facilitate E2-induced growth. After 1 week of growth, mice were imaged using the IVIS Imaging System (Caliper) and stratified into groups of 12 mice each for vehicle and polyamide treatment. Polyamide **1** (25 nmol) in 200 μ L 20% DMSO/PBS was injected subcutaneously into the left shoulder every other day for a total of 4 injections. Vehicle-treated mice received 20%

DMSO/PBS alone. After 3 injections, mice were reimaged. Luciferase output increased an average of 8-fold for the vehicle-treated mice and 3-fold for the mice treated with polyamide 1 (Fig. 3.10A). Mice were euthanized the day following the fourth injection for tumor resection. Tumors from vehicle-treated mice were 71 ± 12 mg and tumors from polyamide-treated mice 55 ± 11 mg (Fig. 3.10B), which does not explain the differences seen in luciferase expression. Representative images of mice treated with polyamide 1 or vehicle at day 6 are shown (Fig. 3.10C).

Effects on ER α -mediated transcription in T47D-KBluc tumor-bearing mice after long-term treatment

To investigate the effects of polyamide 1 in tumor-bearing mice after extended treatment, T47D-KBluc cells were again engrafted into female NSG mice supplemented with a subcutaneous E2 pellet in the right flank. Tumors were grown for 9 days before stratification of 5 mice each into polyamide 1 and vehicle treatment groups. Mice were treated with vehicle or 25 nmol of polyamide 1 in 20% DMSO/PBS, subcutaneously into the left shoulder twice a week for a course of 9 injections (25 days), beginning on day 16 after engraftment (Fig. 3.10D). Treated mice maintained their weights at more than 90% until the final days of treatment when their weights decreased to more than 85% before euthanasia. Luciferase was monitored weekly using the IVIS Imaging System. Luciferase output in the polyamide-treated mice was consistently lower than vehicle-treated mice (Fig. 3.10E). At the experimental endpoint, tumors from vehicle-treated mice were 165 ± 27 mg and tumors from polyamide-treated mice 128 ± 54 mg.

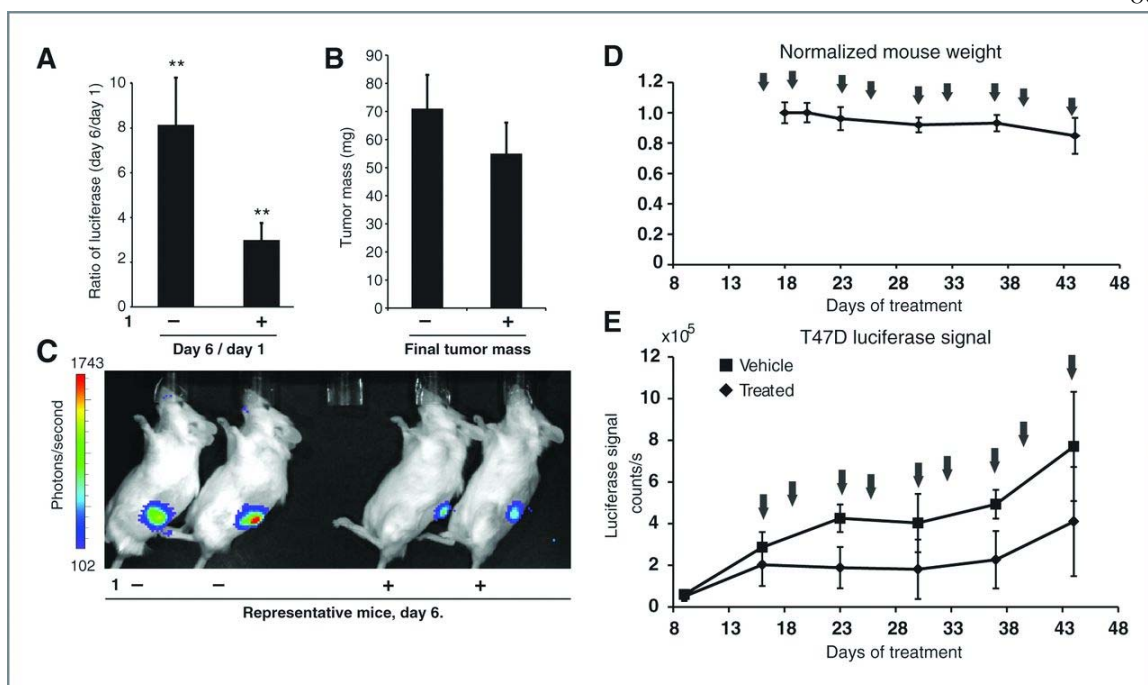


Figure 3.10 Xenograft studies. A, treatment of T47D-KBluc-bearing mice with polyamide 1 results in suppression of ER-driven luciferase. **, $P < 0.01$; $n = 12$ mice per group. Errors are 95% confidence interval (CI). B, tumor masses at experimental endpoint were vehicle: 71 ± 12 mg (95% CI); polyamide 1, 55 ± 11 mg (95% CI). C, representative luciferase output of vehicle and treated mice on day 6. D, treatment schedule for extended time-course experiments with normalized mouse weights over time. Arrows indicate treatment days. E, luciferase signal for polyamide 1 and vehicle-treated groups. Error bars are SDs. Mean tumor masses at the endpoint for animals treated with vehicle is 165 ± 27 mg (95% CI) and for animals treated with 1 is 128 ± 54 mg (95% CI).

Tissue distribution of FITC-conjugated polyamide 5 in mice bearing T47D-KBluc xenografts

Py-Im polyamide 5 is a FITC-labeled conjugate of hairpin **1** that was synthesized to evaluate tissue and subcellular localization via fluorescence microscopy. T47D-KBluc cells cultured *in vitro* and then treated with **5** showed nuclear fluorescence similar to what has been reported in other cell lines (27, 28) treated with FITC-conjugated polyamides in cell culture (Fig. 3.11). An NSG mouse engrafted with T47D-KBluc cells as described in the previous section was treated with polyamide **5** in a manner identical to that of polyamide 1, except at a dose of 50 nmol per injection. After 3 injections, the mouse was euthanized, the tumor resected, and internal organs dissected. Tissue was fixed, cryoprotected, sectioned,

and imaged immediately. Fluorescence signal was evenly distributed throughout multiple sections of the tumor xenograft. A representative section is shown (Fig. 3.12A). High magnification reveals nuclear localization in tumor tissue (Fig. 3.12B). Sections of cardiac muscle show significant cytoplasmic fluorescence in a fibrous pattern (Fig. 3.12C). Sections of kidney and liver both show nuclear fluorescence localization, with minimal cytoplasmic fluorescence (Fig. 3.12D and E). Small bowel epithelia show diffuse cellular fluorescence (Fig. 3.12F).

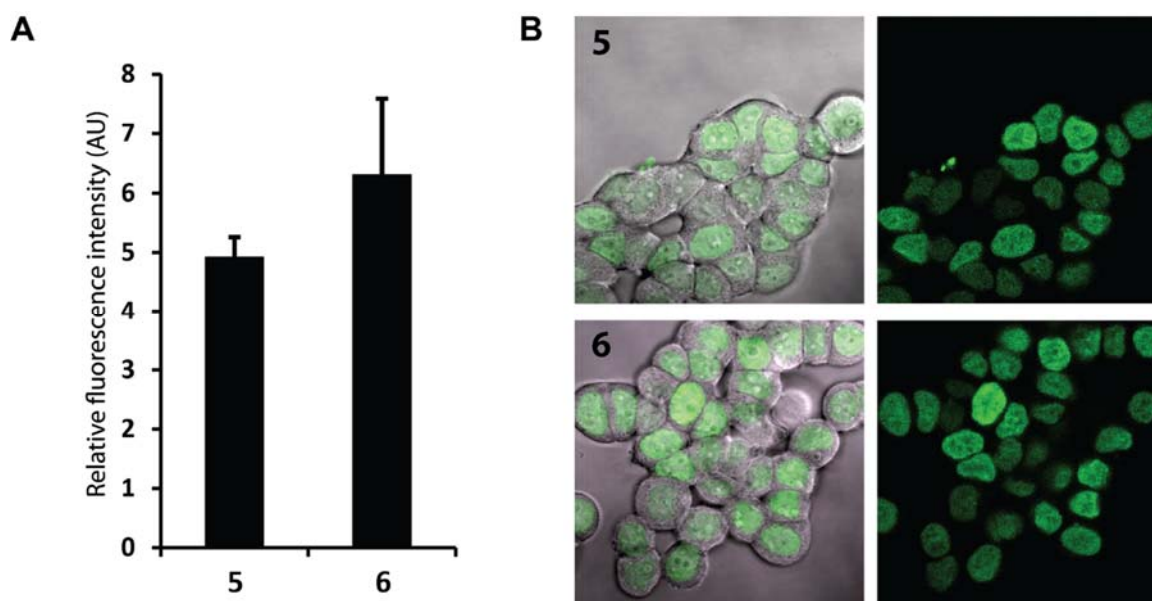


Figure 3.11. Confocal microscopy of live, cultured T47D-KBLUC cells. A, Mean intensity of fluorescence/cell averaged over three images. Errors are 95%CI. B, Representative images of polyamides 5 and 6.

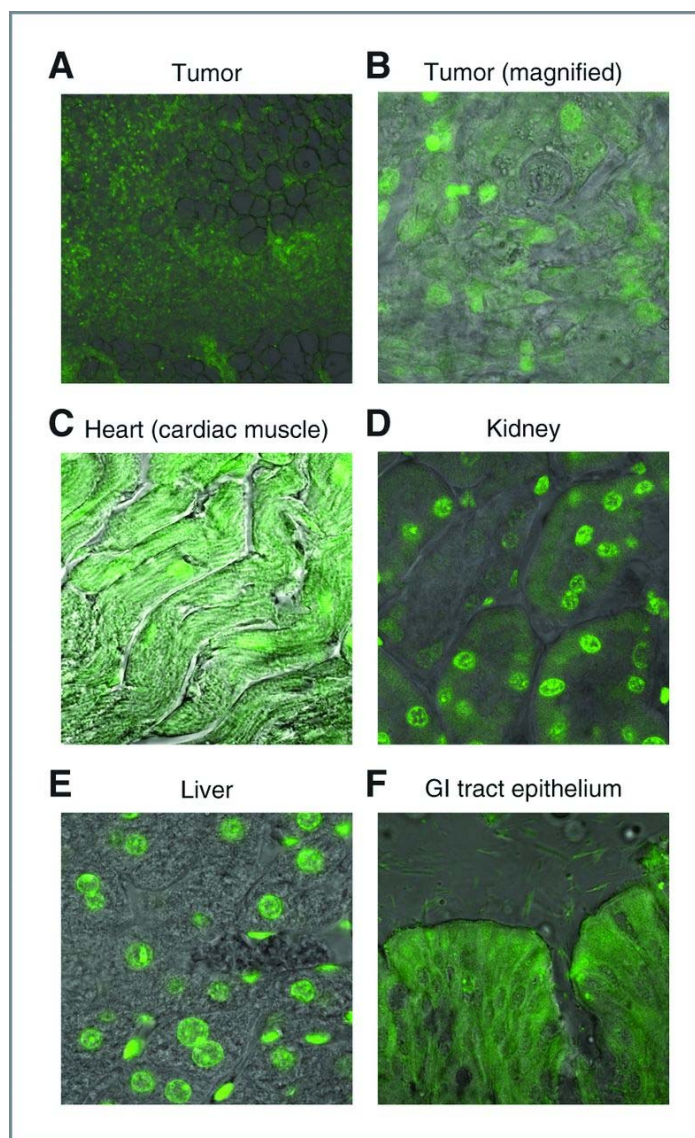


Figure 3.12 Tissue frozen sections of tissue extracted from xenograft-bearing mouse treated with polyamide 5. A, FITC-labeled Py-Im polyamide 5 distributes widely in sections of the T47D-KBluc tumor xenograft. B, high magnification shows nuclear localization of polyamide 5 in tumor cells. C, cardiac muscle sections show a fibrous pattern of fluorescence in the cytoplasm as well as nuclear staining. D, kidneys show nuclear localization of polyamide 5. E, liver sections show nuclear localization of polyamide 5. F, bowel epithelia show cytoplasmic fluorescence. GI, gastrointestinal.

To ensure that nuclear fluorescence in the xenografts was not an artifact of the fixation process, we extracted live cells from T47D-KBluc xenografted tumors from mice treated with polyamide 5 as earlier. In this experiment, cells were isolated via filtration and plated on microscope slides, and incubated for 6 hours before imaging. Cells derived from the tumor showed nuclear staining in a pattern similar to that seen in the fixed tumor sections as well as cultured cells treated with polyamide 5 *in vitro* (Fig. 3.13).

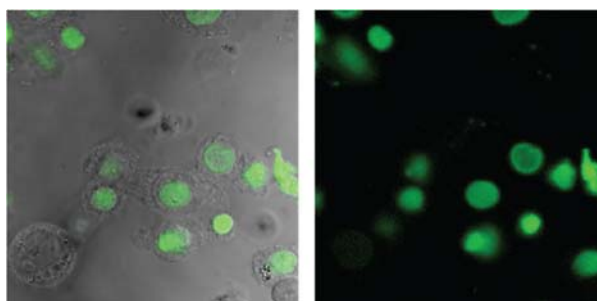


Figure 3.13 Confocal microscopy of live cells taken from T47D-KBLUC xenografts in mice treated with 5.

Discussion

In order for DNA-binding, Py-Im polyamides to be considered for therapeutic application, these molecules must possess favorable pharmacokinetic and pharmacodynamic properties and exert a desired effect in target tissues. In this study, ER α -induced transcription in xenografted breast cancer tumors was the target. A polyamide targeted to the ERE half site 5'-WGGWCW-3' was identified from a focused screen for activity against ER-mediated transcription and cytotoxicity against ER α -positive breast cancer cells. This polyamide was further tested for its global effects on the transcriptome of E2-induced T47D-KBluc cells. Hairpin polyamide 1 showed limited toxicity and circulated at therapeutic levels in serum after subcutaneous injection. It also showed

activity against ER-driven luciferase expression in xenografted tumors in immunocompromised mice. FITC-polyamide conjugate 5 shows widespread localization in body tissues including sections through the xenografted tumor, which reveal nuclear fluorescence.

Suppression of ER-induced gene expression

We screened for both suppression of E2-induced luciferase expression and for antiproliferation by WST-1 assay using T47D-KBluc cells. Polyamide 1 was the most active by both measures, whereas polyamide 3 was inactive by either measure. These molecules differ only at a single atom, which represents the difference between a Py and Im heterocycle. Although polyamides have been shown to have differing uptake properties depending on Py–Im content and sequence (27, 28), the differences in activity in this series is likely not explained by differing uptake efficiency as confocal microscopy of FITC-polyamide conjugates 5 and 6 are similar (Fig. 3.11).

Global effects on the E2-stimulated transcriptome

E2 exerts its effects through direct DNA binding and less frequently extranuclear pathways that do not involve ER α –DNA binding (39). Our genome-wide transcriptome analysis (Fig. 4) revealed that a small fraction of gene expression changes induced by E2 treatment is suppressed by polyamide 1. From a total of 1,003 E2 upregulated genes, only 43 (0.43%) are repressed by polyamide 1 at 1.0 $\mu\text{mol/L}$, and from a total of 575 E2 downregulated genes, 95 (16.5%) were derepressed. However, among the 50 genes most strongly either induced or repressed by E2, a majority were significantly affected by polyamide 1. Among these top 50, 28 (56%) were downregulated by polyamide 1 (1.0

$\mu\text{mol/L}$) at least 2-fold. At a lower cutoff of 1.5-fold, 38 (76%) of E2-induced gene expression changes were abrogated by the action of polyamide 1 at 1.0 $\mu\text{mol/L}$. Many of these strongly E2-responsive genes play important roles in the development of tumors and are therapeutically relevant. Among them is Wilms tumor 1 (*WT1*), a gene originally identified as a tumor suppressor (40); however, more recently it has become apparent that it can also act as an oncogene (41). *WT1* expression is detectable in 90% of breast cancers (42) and high levels of *WT1* expression are correlated with poor patient survival (43). *TFF1* is a predictor for breast cancer patient survival (36). Transforming growth factor- β 2 (*TGF- β 2*) was observed among the most strongly E2-repressed genes and was also over 3-fold derepressed by polyamide 1 at 1.0 $\mu\text{mol/L}$. TGF- β 2 is involved in cancer development that is also derepressed by traditional antiestrogens (44). We conclude that polyamide 1 acts in an antiestrogenic fashion among genes that are most potently affected by E2 but is less active for the majority of E2-responsive genes. If the mechanism by which polyamide 1 interferes with estrogen-driven gene expression is through direct interference with ER–DNA interfaces, we would not expect to affect ER-driven transcription at loci where ER signals through a tethering complex (45), such as with Ap1 and Sp1. Indirect interactions between ER and DNA through tethering with other proteins offer a partial explanation for the limited number of ER-driven transcripts affected by polyamide 1.

Most transcripts affected by polyamide 1 are not explained on the basis of E2 antagonism; 295 genes that are either up- or downregulated by polyamide 1, at least 2-fold that are not explained by effects on ER activity. Of these, 164 are upregulated and 131 downregulated by polyamide 1. To further characterize these effects, we used the DAVID functional annotation tool (46, 47). For the upregulated transcripts, enriched biologic

processes include those involved with the regulation of apoptosis and cell-death, as well as responses to endogenous and hormone stimuli, whereas downregulated genes suggested that polyamide 1 is involved in regulation of GTPase-mediated signal transduction and protein transport and biosynthesis (DAVID database, BP_FAT_GO analysis of genes changed at least 2-fold by treatment with 1 at 1 μ M). The mechanisms of cell death may include the inhibition of transcription (10, 11, 13, 15), but other DNA-dependent processes may contribute and are an area of current investigation. Whether or not the effects of polyamide 1 on these biologic processes are specific to polyamide 1 or may represent a class-effect is unknown but also under study.

Polyamide treatment suppresses E2-simulated luciferase expression in vivo

T47D-KBluc cells were chosen as the cell line for our study based on previous work using T47D cells as a model for ER α -positive breast cancer. Both vehicle- and polyamide-treated groups showed an increase in total luciferase expression from the baseline measurement immediately before treatment on day 1. However, on day 6, after 3 sequential injections, this increase was significantly blunted in the polyamide-treated group as compared with vehicle (from ~8- to 3-fold), suggesting that **1** was able to reach sufficient concentrations in tumor tissue to affect luciferase expression. The approximately 2.5-fold difference in luciferase between polyamide- and vehicle-treated groups, if interpolated to the *in vitro* data, suggest an approximate concentration of 0.3 μ mol/L within the xenograft tissue. Tumor masses did not differ significantly between polyamide- and vehicle-treated mice in this experiment. However, this 6-day experiment may be too brief to adequately assess effects on tumor growth.

Effects on tumor size

Although there are no published reports on the growth of T47D-KBluc xenografts in mice, data from parental T47D xenografts show a slow, linear growth pattern rather than exponential (48). To better assay for antitumor activity of polyamide 1, we conducted similar experiments over a longer period of time. T47D-KBluc xenografted tumors were grown for 2 weeks before initiating treatment, and treatment with polyamide 1 was conducted twice per week for a total of 4 weeks. We observed no significant change in tumor size at the experimental endpoint, although we found a sustained suppression of luciferase output in the polyamide-treated arm as compared with vehicle-treated, consistent with our initial observations. The IC_{50} for cytotoxicity of polyamide 1 in cell culture is 0.47 $\mu\text{mol/L}$, which we believe to be higher than the concentrations achieved within the tumor tissues in this study.

Tissue distribution of FITC-conjugate polyamide 5 in mice after repeated subcutaneous injections

Fixed, frozen sections through multiple internal organs harvested from T47D-KBluc engrafted mice treated with polyamide 5 reveal widespread organ distribution of fluorescent signal but with differing patterns of fluorescence between tissues, and with little obvious systemic toxicity. The tumor sections show nuclear fluorescence in a subcellular pattern that is similar to what is observed in cell culture (Fig. 3.12A). The liver and kidneys also show strong nuclear fluorescence (Fig. 3.12D and E), whereas sections through the intestinal epithelium and cardiac muscle show predominantly cytoplasmic and both cytoplasmic and nuclear fluorescence, respectively. A difference in the cellular uptake

of polyamide–FITC conjugates between cell types has also been observed *in vitro* (27). Recent work has shown that polyamides can form aggregates in solution (49). Whether polyamide aggregation influences distribution *in vivo* is unknown. Tissue-specific targeting of small-molecule drugs is an area of current investigation that may become relevant for this class of molecules as additional *in vivo* experiments are planned.

Conclusion

Polyamide 1 delivered by subcutaneous injection in a simple DMSO/saline vehicle distributed widely in host and tumor tissue and showed adequate bioavailability to affect luciferase expression in xenografted tumor tissue, with acceptable toxicity. Future investigations will include optimization of polyamides for lower systemic toxicity without a compromise in efficacy.

Tables

Table 3.1 Genes induced (or repressed) by either 1 (1 μ M) or E2 (10 nM)Down >2-fold 1.0 μ M PA

AC034193.1
GMD5
TFE1
RALGPS1
TRAPPC9
RP11-1018J8.2
CTD-2313N18.7
SMYD3
RP11-206M11.7
SLC39A11
U6.133
TFE3
EXOC4
DENND1A
AC126407.1
IMMP2L
C11orf49
TIAM1
PDZK1P2
PDZK1P1
PDZK1
PIP
SERPINA6
PCNA
SPINK4
ATG7
CCDC91
DOK7
AE000658.30
CAPSL
PCCA
ACOX2
WT1
SUSD3
RP11-161E22.2
VEPH1
MAP2K5
ATG10
LRBA
KIAA0391
AC010859.1
ADAMT515
COMMD1
ARL15

Up > 2-fold 1.0 μ M PA

GABARAPL1
GABBR1
TROVE2
SLC25A29
GRB7
LZTR1
VEGFA
TNFAIP2
SIRT1
GALT
HIST1H3D
LYPD3
DHX58
PCDH1
PNAFC1B
ENGASE
HES1
MDM4
HIST1H2BD
RPS-857K21.14
NFYB8A
C3orf3
CCNG2
IFRD1
AC011737.2
IL1R1
ZNF251
BAMBI
CC2D1B
PABPC1P10
ZNF302
PARP10
AMOTL2
GGYF1
RP11-169K16.6
OAS1
ESPN
BX322557.10
RP11-434O22.1
RP11-344H11.4
RCN1
SOX4
SLC7A5
ISG15

Up >4-fold 1.0 μ M PA

TGFB2
TNFAIP3
UPK2
ARRDC3

BCKDHB
SERPINA1
RP13-58209.5
RSRC1
TBC1D22A
ELP4
CLSTN2
FAM172A
KIF16B
JPH2
SLC24A3
CUX1
C1orf194
THSD4
PCNXL2
CBARA1
COMMD10
CLPB
TSSC1
RSU1
VPS53
SIPA1L2
ERC1
PIGU
FHL2
MYO1D
RP11-40H20.1
PIGL
MGP
CWC27
TSPAN5
CDC20B
FNI
IQCC
U6.694
OSGIN1
PAM
ITFG1
DEPTOR
AC023161.1
DIP2C
BRE
RBM19
MYEOV
TAB1

ZNF27
PABPC1L
SLC6A9
AMIGO2
TUFT1
PSD4
ADM
PLEKH81
TP53BP1
MEGF6
HSD17B4
C3
PDP1
RARRS53
TXNIP
RPL12P4
LPRN3
PLXNA1
OGT
PTPRU
RPL12P8
RPS-405J24.1
ABCC5
OGFR1
RPS11-154D6.1
CALD1
RPS11-601115.1
AC022007.5
OPLAH
AL132821.1
RP11-373E16.1
HIST2H4B
HIST2H4A
RALGDS
MOSC1
AGA
CLC4
RP11-106M3.1
FAM193B
OSR2
APO05264.1
TMEM44
AC064874.2
NDRG1
AC010487.1
CTS1L

snoU2_19.4
AL132988.3
5_8S_rRNA.6
5100P

E2 >4-fold up

RP11-459E5.1
SPINK4
WT1
TFE1
PDZK1P2
RP11-1018J8.2
DOK7
PDZK1P1
PDZK1
ACOX2
STC2
AREGB
AREG
OLFM1
TFE3
AC135050.3
MYEOV
PTGES
CXCL12
TNS4
SUSD3
NKAIN1
TP53I3
FLT4
LY6E
PEG10
EIF4E1B
LN28A
PFKFB3
GRR3
NMU
RAPGEFL1
SYT12
NCAPG
CAB
GREB1
FH2
AC126407.1
LDHB
IGFBP4
MYC
NPY1R
AL358781.2
RBBP8
MICB
PTTG1
AURKB
GALNT7
SPC24
MCM10

E2 >4-fold down

CDH10
AC005261.1
UPK2
CDHR3
TGFBR2
AQP3
snoU13.267
5_8S_rRNA.6
SOD3
ZDHHC8P1
AL132988.3
RP11-383C5.4
ARL4D
GPRMB
VTCN1
RASL11B
5S_rRNA.486
BCA51
CCDC154
NDRG1
CHST1
CDC42EP3
TRIM29
hsa-mir-1977.1
NANOS1
ELF3
HIST1H4H
UG.1189
UG.1145.10
FGFR4

Down >4-fold 1.0 μ M PA

AC034193.1
GMD5
TFE1
RALGPS1
TRAPPC9
RP11-1018J8.2
CTD-2313N18.7
SMYD3
RP11-206M11.7

RP11-21L23.3
TRBP13
AMZ1
RBP7
LAT2
FAM65C
AGR3
EXO1
DERA
RP11-467L13.5
RRM2
CCNA2
MND1
KCTD6
SPC25
CDCA3
JPH2
DSCC1
NCAPH
MKI67
BIRC5
MGP
CENPA
AGR2
THBS1
DEPDC1B
CDC6
PLK1
KIAA0101
CMTM7
SULF1
PRR11
CDCAS
RRM2P3
NUF2
KIF2C
THSD4
BUB1
AC006465.4
ABCC11
SLC29A1
TROAP
CCNB2
RERG
PKMYT1
CEP55
BUB1B

C9orf117
CDKN2B
CITED2
MAP2
AC114498.3
CCDC159
RPS-1174J21.1
C11orf66
EPAS1
ANXA3
PNPLA7
DUSP1
RPS11-400K9.4
SOX2
CALD1
CSAD
HPX
EPGN
snoU2_19.4
GNMT
BAMBI
TXNIP
HIST1H2AD
J01415.11
IL1R1
HES1
J01415.9
ID3
AL132988.2
L1CAM

PDZK1P2
PDZK1P1
PDZK1
PIP

NDC80
SPAG5
HMMR
WNT10B
NBL1
AC026271.3
TSKU
MELK
TOP2A
SKAP2
SIPA1
MTHFD2
CDC48
DLGAP5
FAM83D
MYBL2
HJURP
ESPL1
GINS1
U6.664
DTL
UHRF1
TNFRSF10C
KIF4A
CDKN3
GNG11
CDC20P1
CDC45
ASF1B
SNCG
KIF4A
RP11-67L3.6
ADCY3
LMNB1
CKAP2L
AURKA
WDR76
PRM1
CASC5
TACC3
CTPS
AL592284.1
HMG2B
RP11-424C20.2
SLC16A3
RPS-1100H13.3
CDC20
SH3BP1
BARD1
NRM
CAT2

AP001816.1
AMT
MALAT1
AC114498.8
CAPSL
AC114498.4
PDP1
NAALADL2
RP11-612B6.2
CD24P4
OSR2
HIST1H2AI
LCN12
MYO1B
AMIGO2
AL713999.8
KCNMA1
LRRC46
COL7A1
snoU13.458
ARMC3
AC064874.2
CPAMD8
AC136698.1
ARHGFE37
RP4-71723.3
C1orf194
MTERFD3
RP11-539L10.3
KIAA1984

KIF11
U6.694
KIFC1
SLC7A1
C1orf97
RP11-467L20.6
KIF20A
TNFRSF10A
AZP1
CCNB1
CDC42
TUBA1B
AC097711.1
FAM72A
NUSAP1
MCM2
PRC1
TK1
TPX2
KIAA1524
CCND1
HINT1
OIP5
UBE2T
C9orf100
C6orf141
FANCI
RP4-774G10.1
GPSM2
CCDC85B
RP11-379F12.3
C9orf100
PCNA
C15orf23
PKC2
DEPOC1
MZT2B
AMD1
C9orf100
OAS3
ARHGAP11A
RP11-336N8.4
RP11-120E5.5
FEN1
RPS-1100H13.3
SNX24
CKS2
NEK2
RP11-417L14.1

Table 3.2 Genes whose induction (or repression) by E2 is inhibited (or repressed by) **1** (1 μ M)

Genes upregulated by E2 >2-fold and downregulated by 1 >2-fold	<p> <i>MYEOV</i> <i>SUSD3</i> <i>AC126407.1</i> <i>THSD4</i> <i>U6.694</i> <i>SERPINA6</i> <i>RP11-206M11.7</i> </p> <p> Genes downregulated by E2 >2-fold and upregulated by 1 >2-fold </p> <p> <i>TGFB2</i> <i>snoU13.267</i> <i>5S_rRNA.486</i> <i>NDRG1</i> <i>hsa-mir-1977.1</i> <i>J01415.10</i> <i>AC114498.3</i> <i>DUSP1</i> <i>CALD1</i> <i>BAMBI</i> <i>TXNIP</i> <i>IL1R1</i> <i>HES1</i> <i>PDP1</i> <i>OSR2</i> <i>AMIGO2</i> <i>AC064874.2</i> <i>SLC25A29</i> <i>SELENBP1</i> <i>TUFT1</i> <i>TP53INP1</i> <i>HIST1H3D</i> <i>RP11-466C23.3</i> <i>OPLAH</i> <i>GPRC5A</i> <i>MEGF6</i> <i>SOX4</i> </p>	<p> <i>J01415.4</i> <i>PSD4</i> <i>AC022007.5</i> <i>CCNG2</i> <i>HIST2H4A</i> <i>HIST2H4B</i> <i>TMEM44</i> <i>MB</i> <i>ZNF251</i> <i>AC010487.1</i> <i>LYPD3</i> <i>PNRC1</i> <i>MTUS1</i> <i>HIST1H2BD</i> <i>LPIN3</i> <i>MTRNR2L2</i> <i>GABBR1</i> <i>ABCC5</i> <i>BX322557.10</i> <i>KLHL24</i> <i>CLK4</i> <i>GABARAPL1</i> <i>FAM193B</i> <i>GRB7</i> <i>RP5-857K21.14</i> <i>AC044860.2</i> <i>ANKRD10</i> <i>C9orf3</i> <i>SCARNA17</i> <i>PLXNA1</i> <i>JDP2</i> <i>HDAC10</i> <i>PABPC1L</i> <i>AMOTL2</i> <i>ZMIZ2</i> <i>LZTR1</i> <i>ESPN</i> <i>RC3H1</i> <i>J01415.19</i> <i>TSPYL2</i> <i>ENGASE</i> </p>	<p> <i>PPAPDC1B</i> <i>J01415.24</i> <i>AC005261.1</i> <i>UPK2</i> <i>AQP3</i> <i>5_8S_rRNA.6</i> <i>AL132988.3</i> <i>RP11-383C5.4</i> <i>RASL11B</i> <i>CDC42EP3</i> <i>ELF3</i> <i>U6.1189</i> <i>RP5-1174J21.1</i> <i>snoU2_19.4</i> <i>HIST1H2AD</i> <i>snoU13.458</i> <i>AC136698.1</i> <i>RP11-539L10.3</i> <i>ARRDC3</i> <i>MTRNR2L9</i> <i>J01415.1</i> <i>ALS93851.1</i> <i>RALGDS</i> <i>PTPRU</i> <i>ATHL1</i> <i>CC2D1B</i> <i>CASP4</i> </p>
---	---	---	--

References

1. Kumar V, Chambon P. The estrogen receptor binds tightly to its responsive element as a ligand-induced homodimer. *Cell* 1988;55:145–56.
2. Manni A, Arafah B, Pearson OH. Estrogen and progesterone receptors in the prediction of response of breast-cancer to endocrine therapy. *Cancer* 1980;46:2838–41.
3. Burstein HJ, Prestrud AA, Seidenfeld J, Anderson H, Buchholz TA, Davidson NE, et al. American Society of Clinical Oncology clinical practice guideline: update on adjuvant endocrine therapy for women with hormone receptor-positive breast cancer. *J Clin Oncol* 2010;28:3784–96. Abstract/FREE Full Text
4. Dervan PB. Molecular recognition of DNA by small molecules. *Bioorg Med Chem* 2001;9:2215–35.
5. Dervan PB, Edelson BS. Recognition of the DNA minor groove by pyrrole-imidazole polyamides. *Curr Opin Struct Biol* 2003;13:284–99.
6. Kielkopf CL, White S, Szewczyk JW, Turner JM, Baird EE, Dervan PB, et al. A structural basis for recognition of A•T and T•A base pairs in the minor groove of B-DNA. *Science* 1998;282:111–5. Abstract/FREE Full Text
7. White S, Baird EE, Dervan PB. On the pairing rules for recognition in the minor groove of DNA by pyrrole-imidazole polyamides. *Chem Biol* 1997;4:569–78.
8. Chenoweth DM, Dervan PB. Allosteric modulation of DNA by small molecules. *Proc Natl Acad Sci U S A* 2009;106:13175–9. Abstract/FREE Full Text
9. Chenoweth DM, Dervan PB. Structural basis for cyclic Py–Im polyamide allosteric inhibition of nuclear receptor binding. *J Am Chem Soc* 2010;132:14521–9.

10. Muzikar KA, Nickols NG, Dervan PB. Repression of DNA-binding dependent glucocorticoid receptor-mediated gene expression. *Proc Natl Acad Sci U S A* 2009;106:16598–603. Abstract/FREE Full Text
11. Nickols NG, Dervan PB. Suppression of androgen receptor-mediated gene expression by a sequence-specific DNA-binding polyamide. *Proc Natl Acad Sci U S A* 2007;104:10418–23. Abstract/FREE Full Text
12. Raskatov JA, Meier JL, Puckett JW, Yang F, Ramakrishnan P, Dervan PB. Modulation of NF-kappa B-dependent gene transcription using programmable DNA minor groove binders. *Proc Natl Acad Sci U S A* 2012;109:1023–8. Abstract/FREE Full Text
13. Nickols NG, Jacobs CS, Farkas ME, Dervan PB. Modulating hypoxia-inducible transcription by disrupting the HIF-1-DNA interface. *ACS Chem Biol* 2007;2:561–71.
14. Olenyuk BZ, Zhang GJ, Klco JM, Nickols NG, Kaelin WG, Dervan PB. Inhibition of vascular endothelial growth factor with a sequence-specific hypoxia response element antagonist. *Proc Natl Acad Sci U S A* 2004;101:16768–73. Abstract/FREE Full Text
15. Yang F, Nickols NG, Li BC, Marinov GK, Said JW, Dervan PB. Antitumor activity of a pyrrole-imidazole polyamide. *Proc Natl Acad Sci U S A* 2013;110:1863–8. Abstract/FREE Full Text
16. Fukasawa A, Aoyama T, Nagashima T, Fukuda N, Ueno T, Sugiyama H, et al. Pharmacokinetics of pyrrole-imidazole polyamides after intravenous administration in rat. *Biopharm Drug Dispos* 2009;30:81–9.
17. Nagashima T, Aoyama T, Fukasawa A, Watabe S, Fukuda N, Ueno T, et al. Determination of pyrrole-imidazole polyamide in rat plasma by liquid chromatography-tandem mass spectrometry. *J Chromat B: Biomed Sci Appl* 2009;877:1070–6. Caltech ConnectCrossRefGoogle Scholar

18. Nagashima T, Aoyama T, Yokoe T, Fukasawa A, Fukuda N, Ueno T, et al. Pharmacokinetic modeling and prediction of plasma pyrrole-imidazole polyamide concentration in rats using simultaneous urinary and biliary excretion data. *Biol Pharm Bull* 2009;32:921–7.
19. Matsuda H, Fukuda N, Ueno T, Katakawa M, Wang X, Watanabe T, et al. Transcriptional inhibition of progressive renal disease by gene silencing pyrrole-imidazole polyamide targeting of the transforming growth factor-beta 1 promoter. *Kidney Int* 2011;79:46–56.
20. Raskatov JA, Nickols NG, Hargrove AE, Marinov GK, Wold B, Dervan PB. Gene expression changes in a tumor xenograft by a pyrrole-imidazole polyamide. *Proc Natl Acad Sci U S A* 2012;109:16041–5. [Abstract/FREE Full Text](#)
21. Gearhart MD, Dickinson L, Ehley J, Melander C, Dervan PB, Wright PE, et al. Inhibition of DNA binding by human estrogen-related receptor 2 and estrogen receptor alpha with minor groove binding polyamides. *Biochemistry* 2005;44:4196–203.
22. White S, Szewczyk JW, Turner JM, Baird EE, Dervan PB. Recognition of the four Watson–Crick base pairs in the DNA minor groove by synthetic ligands. *Nature* 1998;391:468–71.
23. Nickols NG, Jacobs CS, Farkas ME, Dervan PB. Improved nuclear localization of DNA-binding polyamides. *Nucleic Acids Res* 2007;35:363–70. [Abstract/FREE Full Text](#)
24. Synold TW, Xi B, Wu J, Yen Y, Li BC, Yang F, et al. Single-dose pharmacokinetic and toxicity analysis of pyrrole-imidazole polyamides in mice. *Cancer Chemother Pharmacol* 2012;70:617–25.
25. Wilson VS, Bobseine K, Gray LE. Development and characterization of a cell line that stably expresses an estrogen-responsive luciferase reporter for the detection of estrogen receptor agonist and antagonists. *Toxicol Sci* 2004;81:69–77. [Abstract/FREE Full Text](#)
26. Puckett JW, Green JT, Dervan PB. Microwave assisted synthesis of Py–Im polyamides. *Org Lett* 2012;14:2774–7.

27. Best TP, Edelson BS, Nickols NG, Dervan PB. Nuclear localization of pyrrole-imidazole polyamide-fluorescein conjugates in cell culture. *Proc Natl Acad Sci U S A* 2003;100:12063–8. Abstract/FREE Full Text
28. Edelson BS, Best TP, Olenyuk B, Nickols NG, Doss RM, Foister S, et al. Influence of structural variation on nuclear localization of DNA-binding polyamide-fluorophore conjugates. *Nucleic Acids Res* 2004;32:2802–18. Abstract/FREE Full Text
29. Nowak DE, Tian B, Brasier AR. Two-step cross-linking method for identification of NF-kappa B gene network by chromatin immunoprecipitation. *Biotechniques* 2005;39:715–25.
30. Raskatov JA, Hargrove AE, So AY, Dervan PB. Pharmacokinetics of Py-Im polyamides depend on architecture: cyclic versus linear. *J Am Chem Soc* 2012;134:7995–9.
31. Langmead B, Trapnell C, Pop M, Salzberg SL. Ultrafast and memory-efficient alignment of short DNA sequences to the human genome. *Genome Biol* 2009;10:R25.
32. Anders S, Huber W. Differential expression analysis for sequence count data. *Genome Biol* 2010;11:R106.
33. Welboren WJ, van Driel MA, Janssen-Megens EM, van Heeringen SJ, Sweep FCGJ, Span PN, et al. ChIP-Seq of ER alpha and RNA polymerase II defines genes differentially responding to ligands. *EMBO J* 2009;28:1418–28.
34. Stabile LP, Lyker JS, Gubish CT, Zhang W, Grandis JR, Siegfried JM. Combined targeting of the estrogen receptor and the epidermal growth factor receptor in non-small cell lung cancer shows enhanced antiproliferative effects. *Cancer Res* 2005;65:1459–70. Abstract/FREE Full Text
35. Lau KM, LaSpina M, Long J, Ho SM. Expression of estrogen receptor (ER)-alpha and ER-beta in normal and malignant prostatic epithelial cells: regulation by methylation and involvement in growth regulation. *Cancer Res* 2000;60:3175–82. Abstract/FREE Full Text

36. Le Page Y, Scholze M, Kah O, Pakdel F. Assessment of xenoestrogens using three distinct estrogen receptors and the zebrafish brain aromatase gene in a highly responsive glial cell system. *Environ Health Perspect* 2006;114:752–8. Caltech ConnectMedlineGoogle Scholar
37. Devidze N, Fujimori K, Urade Y, Pfaff DW, Mong JA. Estradiol regulation of lipocalin-type prostaglandin D synthase promoter activity: evidence for direct and indirect mechanisms. *Neurosci Lett* 2010;474:17–21.
38. Trapnell C, Roberts A, Goff L, Pertea G, Kim D, Kelley DR, et al. Differential gene and transcript expression analysis of RNA-seq experiments with TopHat and Cufflinks. *Nat Protoc* 2012;7:562–78.
39. Madak-Erdogan Z, Kieser KJ, Kim SH, Komm B, Katzenellenbogen JA, Katzenellenbogen BS. Nuclear and extranuclear pathway inputs in the regulation of global gene expression by estrogen receptors. *Mol Endocrinol* 2008;22:2116–27.
40. Little M, Wells C. A clinical overview of WT1 gene mutations. *Hum Mutat* 1997;9:209–25.
41. Yang L, Han Y, Saurez Saiz F, Minden MD. A tumor suppressor and oncogene: the WT1 story. *Leukemia* 2007;21:868–76. Caltech ConnectMedlineGoogle Scholar
42. Loeb DM, Evron E, Patel CB, Sharma PM, Niranjana B, Buluwela L, et al. Wilms' tumor suppressor gene (WT1) is expressed in primary breast tumors despite tumor-specific promoter methylation. *Cancer Res* 2001;61:921–5. Abstract/FREE Full Text
43. Miyoshi Y, Ando A, Egawa C, Taguchi T, Tamaki Y, Tamaki H, et al. High expression of Wilms' tumor suppressor gene predicts poor prognosis in breast cancer patients. *Clin Cancer Res* 2002;8:1167–71. Abstract/FREE Full Text
44. Foekens JA, Rio MC, Seguin P, Vanputten WLJ, Fauque J, Nap M, et al. Prediction of relapse and survival in breast-cancer patients by PS2 protein status. *Cancer Res* 1990;50:3832–7. Abstract/FREE Full Text

45. Stender JD, Kim K, Charn TH, Komm B, Chang KC, Kraus WL, et al. Genome-wide analysis of estrogen receptor alpha DNA binding and tethering mechanisms identifies Runx1 as a novel tethering factor in receptor-mediated transcriptional activation. *Mol Cell Biol* 2010;30:3943–55. [Abstract/FREE Full Text](#)
46. Huang da W, Sherman BT, Lempicki RA. Systematic and integrative analysis of large gene lists using DAVID bioinformatics resources. *Nat Protoc* 2009;4:44–57.
47. Huang da W, Sherman BT, Lempicki RA. Bioinformatics enrichment tools: paths toward the comprehensive functional analysis of large gene lists. *Nucleic Acids Res* 2009;37:1–13. [Abstract/FREE Full Text](#)
48. Ishii Y, Waxman S, Germain D. Tamoxifen stimulates the growth of cyclin D1—overexpressing breast cancer cells by promoting the activation of signal transducer and activator of transcription 3. *Cancer Res* 2008;68:852–60. [Abstract/FREE Full Text](#)
49. Hargrove AE, Raskatov JA, Meier JL, Montgomery DC, Dervan PB. Characterization and solubilization of pyrrole-imidazole polyamide aggregates. *J Med Chem* 2012;55:5425–32.